Remote Sensing of Environment 121 (2012) 335–346

Contents lists available at SciVerse ScienceDirect

Remote Sensing of Environment

journal homepage: www.elsevier.com/locate/rse

Multi sensor validation and error characteristics of Arctic satellite sea surface temperature observations

Jacob L. Høyer [a,*], Ioanna Karagali [b], Gorm Dybkjær [a], Rasmus Tonboe [a]

[a] Centre for Ocean and Ice, Danish Meteorological Institute, Lyngbyvej 100, DK-2100, Copenhagen, Denmark
[b] Wind Energy Division, Risø National Laboratory for Sustainable Energy, Technical University of Denmark, Frederiksborgvej 399, Building 125, DK-4000, Roskilde, Denmark

ARTICLE INFO

Article history:
Received 26 May 2011
Received in revised form 22 December 2011
Accepted 15 January 2012
Available online 22 March 2012

Keywords:
Arctic
SST
Validation
Error characteristics
Marginal ice zone

ABSTRACT

Six of the operational global satellite sea surface temperature products from infrared and microwave sensors are validated in a consistent way in waters north of 60° N. The 15-month validation with drifting buoy in situ observations shows that data from the Advanced Along-Tracking Scanning Radiometer (AATSR) on-board the ENVISAT satellite and NAVOCEANO data from the Advanced Very High Resolution Radiometer (AVHRR) on-board the NOAA 18 satellite are superior in terms of bias and standard deviation. The observations from the Advanced Microwave Scanning Radiometer-EOS (AMSR-E) on-board the Aqua satellite have superior coverage due to the microwaves' ability to penetrate cloud cover.

The performance of the different satellite products is examined for variation with season, water temperature, solar elevation angle, and proximity to the marginal ice zone. The validation results identify errors in the satellite products related to observation techniques, data processing and cloud masking. Temporal and spatial error scales are derived for all satellite products using the satellite versus in situ match-up dataset. Temporal error scales are typically between 1 and 2 days and the characteristic spatial error scales between 300 and 500 km. The error cross correlations between the different satellite products reveal that the products from the infrared sensors generally show significant error correlation, whereas the errors of the microwave AMSR-E product have a low correlation with all the products from the infrared sensors.

1. Introduction

Sea surface temperature (SST) observed from satellite is an important parameter, which can be used for climate change detection, air–sea heat flux calculations and assimilation into ocean and atmospheric models (e.g., Carton et al., 2000; Rayner, et al., 2003). The Arctic Ocean is one of the world's most important oceanic regions for observing and modeling. The decrease in sea ice extent in recent years, with the 2007 record low 38% below the climatological mean (Comiso et al., 2008), has increased the open water areas, particularly during summer and fall. In addition, climate models suggest that a positive ice-albedo feedback related to loss of sea ice leads to an Arctic amplification of the global warming (Lindsay & Zhang, 2005; Walsh et al., 2002). It is therefore essential to document and characterize the errors of the satellite SST observations in the Arctic Ocean in order to support proper assimilation into ocean/atmosphere models and for climate change detection.

The high latitudes, including the Arctic Ocean, are recognized by the satellite SST community to be a challenging region for retrieval of accurate SST observations (Donlon et al., 2010). In the Arctic Ocean, there are several factors that complicate the retrieval of SST and cloud detection. The infrared (IR) retrieval algorithms have been tuned on global datasets to correct for the effect of water vapor (e.g., Barton, 1995). However, the atmosphere in the Arctic Ocean is normally very dry, which can result in an overcompensation by the global SST algorithms (Vincent et al., 2008a, 2008b). Furthermore, a persistent cloud cover, and extended twilight periods makes it difficult for the cloud detection algorithms to identify clouds correctly. In addition, the presence of large areas with mixed sea ice and open water complicates the retrieval of SST. Finally, due to sea ice and inaccessibility, the amount of in situ observations for validating satellite observations at high latitudes is limited compared to other regions of the world. These factors, and the fact that no systematic validation and error characterization study has been made specifically for the high latitudes, result in a general uncertainty concerning the quality of the satellite SST observations in the Arctic.

Several satellite producers have developed their own individual match-up datasets (MD), to compare coincident in situ and satellite observations for calibration and validation of their satellite products. As the match-up datasets are used for validating and improving the specific retrieval algorithms, the criteria for constructing the match-up datasets vary from one producer to the other. This renders intercomparisons based upon different MDs difficult.

* Corresponding author. Tel.: +45 39157203.
E-mail address: jlh@dmi.dk (J.L. Høyer).

0034-4257/$ – see front matter © 2012 Elsevier Inc. All rights reserved.
doi:10.1016/j.rse.2012.01.013

In this paper, we perform a systematic validation and error characterization of several of the satellite SST products that are most frequently used at high latitudes. They cover IR and microwave (MW) observations with spatial resolutions from 1 to more than 50 km and comprise data from six polar orbiting satellites. The spatial and temporal scales of the errors on the satellite products are presented together with the cross correlation of the errors on different satellite SST products.

The paper is structured with an introduction to the study area and the in situ and satellite data used in this study (Section **2**), followed by sections describing the match-up limits (Section **3**) and the general error statistics (Section **4**). Section **5** presents the error scales and the error correlations between the different satellite products followed by Section **6** that examines the errors in the marginal ice zone. Finally, Section **7** contains our concluding remarks.

2. Observations

2.1. Study area

The study will focus on satellite SST observations north of 60° N, and the performance of the satellite SST products in the marginal ice zone. The validation area covers a range of different oceanographic conditions including the inflow to the Nordic Seas of the waters in the North Atlantic Current with warm (5–12 °C) and salty (35–35.3 on the practical salinity scale) waters. In addition, the inner Arctic Ocean (> 80° N) is influenced by fresh water input from large rivers generating a surface layer with salinities as low as 30 parts per thousands in the Canadian Basin (e.g., Tomczak, & Godfrey, 1994).

The atmospheric circulation in the area is dominated by the persistent high pressure close to the North Pole and by the influence from the storm tracks in the southern Nordic seas near Iceland and the Faroe Islands. The easterly winds over the inner Arctic generate an anticyclonic circulation, which exports cold and low salinity water and ice southward through the Fram Strait (Tomczak & Godfrey, 1994). The annual mean specific humidity at the surface ranges from more than 4 g/kg in the Norwegian seas to less than 2 g/kg north of 80° N. The Arctic is dominated by a persistent cloud cover for up to 90% of the time during summer and 50–60% of the time during winter (Peixoto & Oort, 1992).

A seasonal and a perennial ice cover influence the majority of the validation area. This is illustrated in Fig. 1, which shows the number of days with ice cover in the Arctic during a year. The ice information is from the EUMETSAT Ocean and Sea Ice Satellite Application Facility (OSI-SAF).

2.2. In situ observations

The in situ observations consist of SST observations from drifting surface buoys that are reporting observations on an hourly basis. The drifting buoy observations are superior to observations made from ships measuring the temperature at the water intake in the hull (Emery et al., 2001; Poulter & Eastwood, 2008) and are used for several global and regional validation studies (Harris and Saunders, 1996; Corlett, et al., 2006). The temperature sensor on the drifting buoys is placed at a depth of approximately 20 cm (see e.g. http://www.jcommops.org/dbcp/community/standards.html) and the observations have an error of about 0.2 °C (O'Carroll et al., 2008). The spatial and temporal distribution of the buoy observations are shown in Fig. 2.

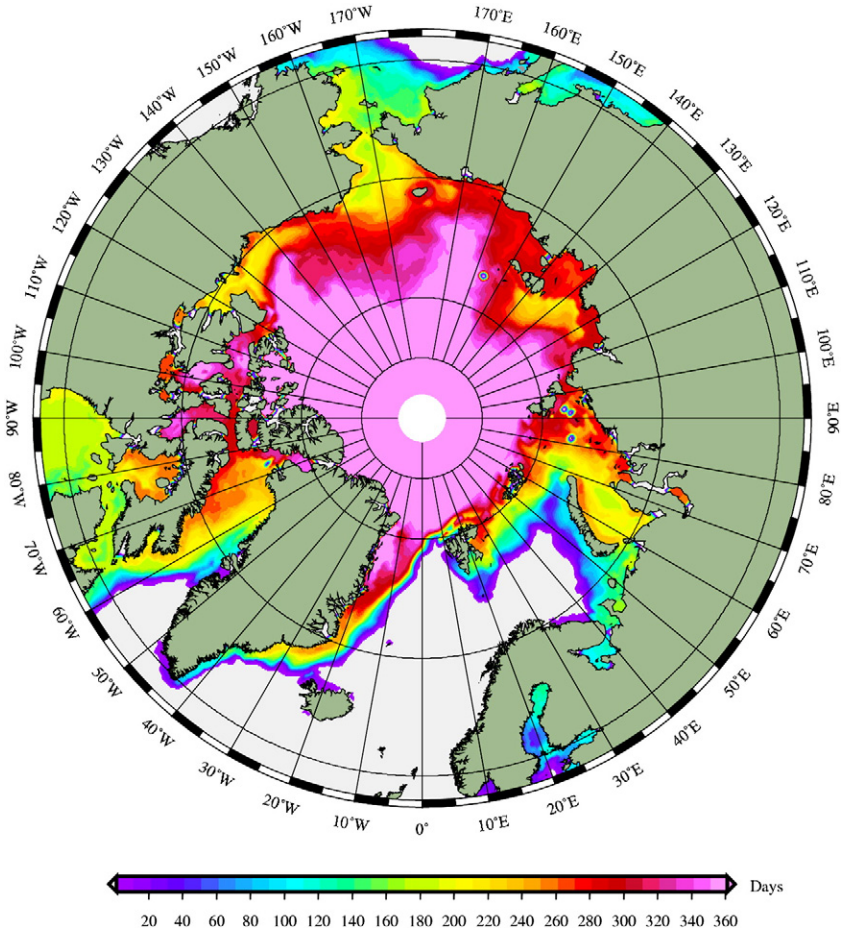

Fig. 1. Number of days with ice cover during one year (November 2009 to November 2010).

Fig. 2 reveals an uneven spatial distribution of the buoy observations. Due to the extension of the ice cover and to difficult navigation in ice filled waters, the number of in situ observations at high latitudes is small compared to the number at mid-latitudes. Thus, the large majority of observations come from the Nordic seas, the Barents Sea and the Chukchi Sea, whereas no observations have been reported from the Baffin Bay and the Russian part of the Arctic Ocean. About 88% of the in situ observations come from within the longitudes 50° W and 50° E. Additional observations from other sources are available, e.g. moored buoys in the Barents Sea. These have not been included in this study due to their different error characteristics. In addition, the moored buoys are located in positions in the Barents Sea, where many drifting buoys are also reporting.

The data have been obtained from the Coriolis data center (http://www.coriolis.eu.org) for the 15-month period, from November 2009 to February 2011. Preliminary quality control was done by the Coriolis data center. We applied three additional quality checks: gross error, redundancy and climatology. The gross error check removed in situ observations lower than −1.8 °C or higher than 35 °C. The redundancy check identified in situ observations within 0.005° in space, 0.15 °C in temperature and 15 min in time. Only one observation was allowed within these limits and additional observations were discarded. Finally, a climatology check removed in situ observations deviating more than −2 and +3 °C from the Pathfinder V5.0 nighttime climatology (e.g., Casey & Cornillon, 1999). The asymmetry in the climatology check arises from the climate being about 0.5–1 °C colder

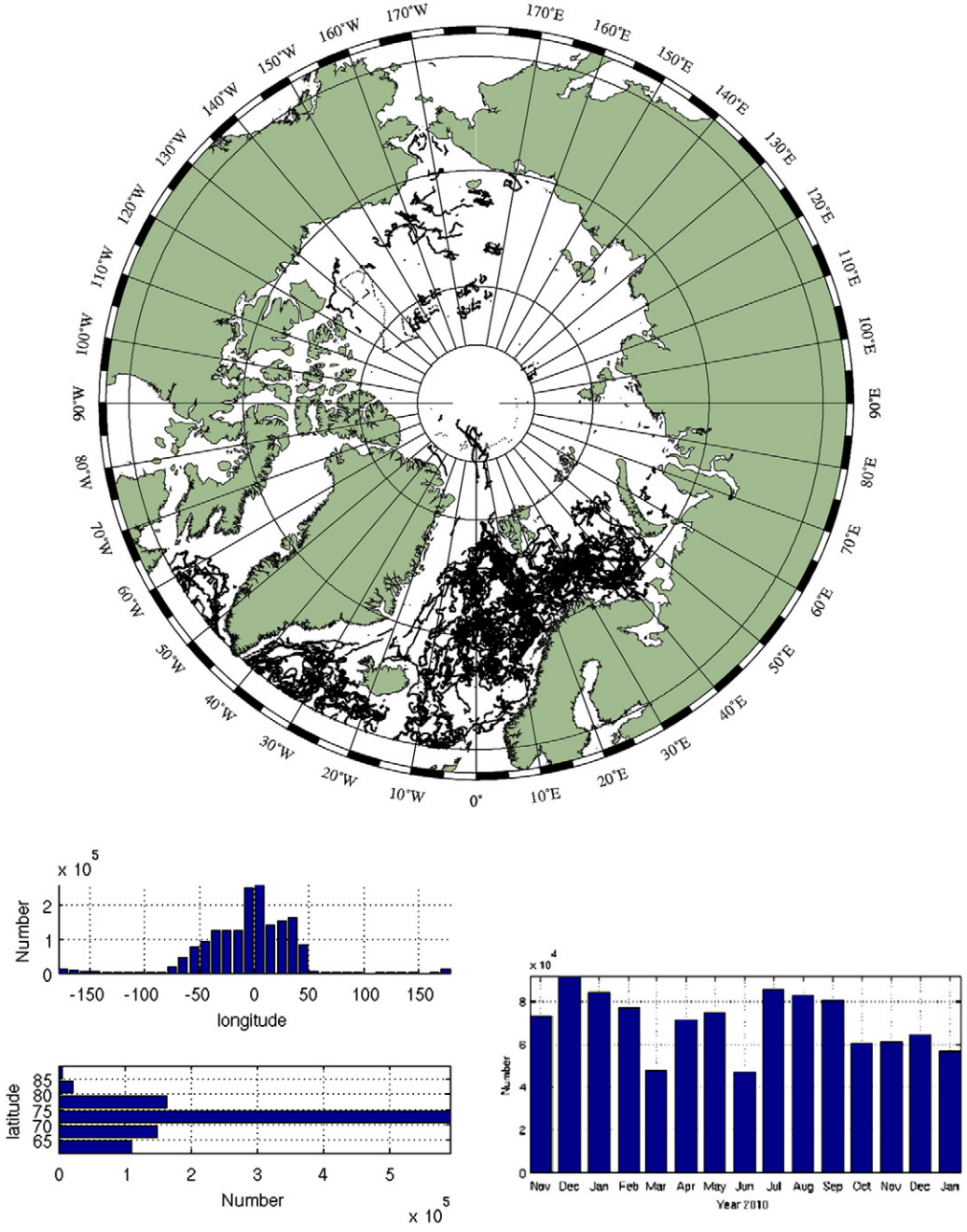

Fig. 2. Distribution of buoy observations in the study area from November 2009 to February 2011. The top figure shows the spatial distribution of all the in situ observations, whereas the lower left figures show the longitudinal and latitudinal distribution of the in situ observations binned in 10° longitude and 5° latitude, respectively. The lower right figure shows the monthly number of in situ observations throughout the validation period.

than the observations during this period. The gross error, redundancy and climatology checks removed 0.3%, 10.6% and 3.2% of the observations, respectively.

Observations were discarded if any of the tests failed. The percentage of discarded in situ observations in the climatology check was similar for the different satellite products and no preference was found towards the AVHRR products. Due to technical reasons, only a limited amount of observations were available from the Coriolis Data centre during May 2010. Instead we used data from the Global Telecommunications Systems (GTS) for the month of May. These data were subjected to the same quality control as the rest of the dataset.

It is evident from Figs. 1 and 2 that a few buoys report SST from ice covered areas. These observations have been discarded from the comparisons with satellite observations later, using auxiliary ice concentration data.

2.3. Satellite observations

The data used for this study were provided in the GHRSST L2P format (Donlon et al., 2007). The different satellite SST products and their characteristics are listed in Table 1 and cover high resolution IR and coarse resolution MW satellite observations. Note that the data grid of the satellite SST product may not equal the actual resolution of the SST observations. The AMSR-E MW SST algorithm e.g. include observations from the 6.9 GHz channel that has a footprint of 76×44 km (see e.g., Wentz & Meissner, 2007, Gentemann et al., 2010), which is much larger than the data grid of 25 km.

The NOAA 18 AVHRR data are processed by the Naval Oceanographic Office, Stennis Space Center, MS, USA and obtained from the JPL Global Data Assembly Centre (GDAC, ftp://podaac.jpl.nasa.gov/GHRSST/data/L2P/). For details on the retrieval algorithm and data processing, see May, et al., 1998. The product is a Global Area Coverage (GAC) and it is therefore abbreviated NAVO-GAC in the rest of the paper. The AATSR ENVISAT data have been provided by the European Space Agency (ESA), and processed by the UK Multi-Mission Product Archive Facility (UK-MM-PAF) on behalf of ESA. For performance and algorithm descriptions, see Corlett, et al., 2006 and http://envisat.esa.int/dataproducts/aatsr/ for product handbooks. The Metop-A AVHRR data have been processed by Centre Meteorological Spatiale (CMS) for the OSI-SAF project (http://www.osi-saf.org). The algorithm is documented in: O&SI SAF Project Team, 2010 and obtained from ftp://ftp.ifremer.fr. MODIS data from the Aqua and Terra platforms have been processed jointly by NASA Jet Propulsion Laboratory, NASA Ocean Biology Processing Group and University of Miami Rosential School of Atmospheric and Marine Science (NASA/JPL/OBPG/RSMAS, see e.g., Brown et al., 1999), and obtained from the GDAC. Here, the MODIS Aqua data are abbreviated MODIS whereas the MODIS Terra data are abbreviated MODIST. The AMSR-E data have been processed and provided by the Remote Sensing Systems (Wentz & Meissner, 2000, 2007, http://www.ssmi.com/). All L2P products have been obtained as part of the operational DMI-OI level 4 processing chain (see e.g. Høyer & She, 2007).

The SST retrieval algorithms for the individual satellite products will not be described in detail here, but the IR satellite products are based upon the multichannel linear and nonlinear algorithms see (e.g., Barton, 1995; McClain et al., 1985; Walton et al., 1998). During daytime, the nonlinear algorithm takes the form of

$$SST = a + bT_4 + c\,(T_4 - T_5)T_{guess} + d(T_4 - T_5)(\sec\theta - 1) \quad (1)$$

where T_4 and T_5 represent the brightness temperature for channels 4 and 5, respectively and T_{guess} is a first guess temperature from e.g. climatology. a, b, c and d are coefficients determined in the calibration of the algorithm and θ is the satellite zenith angle. The nighttime algorithms typically include observations from channel 3 (T_3) through the additional term: $e(\sec\theta - 1)T_3$. Setting T_{guess} to unity will reduce the equation to the standard linear algorithm.

All the IR algorithms thus use the difference between two spectral bands in the thermal infrared to account for water vapor effects, and they provide a skin or subskin SST value depending upon, whether in situ observations or radiative transfer modeling has been used to tune the parameters in the algorithm (Merchant et al., 1999; Zavody, et al., 1995). All the IR algorithms use the two channels algorithm type during daytime and the three channels type during nighttime.

The technique for SST retrievals in the microwave part of the spectrum is fundamentally different (see e.g. Wentz & Meissner, 2000, 2007). MW radiometer observations of the sea surface are corrected for sea surface roughness and atmospheric attenuation. Data influenced by precipitation are discarded.

The GHRSST SST products follow the GHRSST Data Processing Specification (GDS), which requires the L2P data products to include a quality flag (proximity_confidence) that ranges from 0 to 5, where 0 is bad and 5 is excellent (see e.g. Donlon et al., 2007). Only satellite observations with quality flags 4 and 5 are included in this study. In this range, the AMSR-E SST data only use the value 4 for good data. Metop-A observations had no quality flag 5 values before June 2010 due to the absence of aerosol information (P. LeBorgne, pers. comm., 2010). The validated data field is called sea_surface_temperature in the data file for all the products, except for the MODIS Aqua and Terra products. For both MODIS products the variable is called sst4, which is nighttime observations including the 4 μm satellite channel. The GHRSST satellite producers supply single sensor error statistics (SSES) to the observations. These biases are provided by the satellite producers as the best estimate of the bias on the satellite retrieval algorithms. They have been subtracted from the products as recommended by Donlon et al., 2007. Observations from the low- and mid-latitudes have shown that the cool surface skin effect on average makes the water surface about 0.17 K colder than the subskin surface water (e.g., Donlon et al., 2002; Schluessel et al., 1987). Algorithms using in situ observations to determine the parameters in Eq. (1) are providing subskin SST observations, as the cool skin effect is not included in standard in situ observations.

The satellite products in Table 1 provide SST at the subskin level except for the MODIS Aqua and Terra and the AATSR products, which are provided as skin SST. To validate all satellite products in a consistent way, an offset of 0.17 °C has been added to the skin satellite products (Donlon et al., 2002). All the results in this paper are subsequently understood as subskin satellite SST observations.

Table 1
Characteristics of the infrared (IR) and microwave (MW) satellite observations used in the study, see the text for more details on the data providers.

Product name	Data provider	Satellite	Sensor	Observation technique	Data grid (km)
NAVO-GAC	Naval Oceanographic Office, USA	NOAA 18	AVHRR	IR	9
AATSR	ESA/UK-MM-PAF	ENVISAT	AATSR	IR	1
Metop-A	OSI-SAF/Meteo France	Metop-A	AVHRR	IR	1
MODIS	NASA/JPL/OBPG/RSMAS	Aqua	MODIS	IR	1
MODIST	NASA/JPL/OBPG/RSMAS	Terra	MODIS	IR	1
AMSR-E	Remote Sensing Systems	Aqua	AMSR-E	MW	25

As mentioned earlier, the seasonal variations in the oceanic and atmospheric conditions in the Arctic are very large (Peixoto & Oort, 1992). Therefore, it is important to carry out the validation for at least one full year to cover the seasonal variations in the validation results related to changes in the atmospheric and oceanic conditions. In comparisons with in situ observations, the standard deviation in errors for the global IR satellite observations typically range from 0.3 to 0.5 °C (O'Carroll et al., 2006, Corlett et al., 2006,), whereas the MW observations lie within 0.6 °C (Wentz et al., 2000). However, it is well known that regional errors may exceed these numbers (see e.g. Chan & Gao, 2005).

3. Match-up data set

A match-up data set has been compiled by pairing satellite and in situ observations within certain spatial (Δx) and temporal (Δt) windows. Based on previous experiences, a match-up pair of in situ and satellite observations is selected when the satellite observation is within 15 km of the in situ observation, and when the two observations are within 2 h of each other. Only satellite observations with quality flags 4 or higher and satellite-in situ differences of less than 10 °C are used. The minimum distance from the in situ observations to the ice edge is calculated using the OSI-SAF northern hemisphere ice edge product on a 10 km polar stereographic grid.

The total number of match-up pairs for each product depends on the number of in situ observations, the spatial resolution, cloud cover (for IR products) and the coverage of the satellite sensor. The highest number of match-up pairs is found for the MODIS Aqua and Terra products, and the lowest number of match-up pairs is found for the NAVO-GAC product. The statistics are shown in Table 2 and are discussed in the next section.

The differences between satellite and in situ observations include contributions from errors in the buoy observations, errors on the satellite observations and sampling errors introduced through the differences in sampling characteristics and the distance in space and time between the match-up pairs.

The error budget is

$$\varepsilon^2_{\mathrm{Diff}} = \varepsilon^2_{\mathrm{Buoy}} + \varepsilon^2_{\mathrm{Satellite}} + \varepsilon^2_{\mathrm{Sampling}} \quad (2)$$

Where the error variances for the respective contributions are added (see e.g. Emery and Thomson, 1998). The errors arising from the fact that the satellite and in situ observations are not coinciding in space and time are seen in Fig. 3, where the error statistics are shown as a function of the size of the match-up windows Δx and Δt. The results are from the AATSR satellite and indicate that the variability introduced by spatial differences can be significant for Δx larger than about 5 km, and that the biases do not change significantly between 1 km and 15 km. The number of match-ups within 1 km is in general about 2–4% of the number of match-ups within 5 km. If the center pixel is cloudy, match-ups away from center pixel may become cloud contaminated match-ups. However, the expected cold bias from this effect is insignificant, as seen from Fig. 3 (left).

Variations in Δt do not influence the standard deviations significantly for match-up differences less than 120 min. An asymmetry is found in the daytime bias (Fig. 3, right). This systematic bias variation is probably related to diurnal temperature variations (e.g., Eastwood et al., 2011; Gentemann et al., 2008) and the effect is also found in global validation studies (Embury et al., 2012). The signal is consistent with the Sun-synchronous satellite passing times in the morning and diurnal variability of the ocean. An in situ observation after the satellite observation will thus tend to be warmer due to the diurnal warming.

The other IR satellites show similar patterns with the spatial and temporal match-up differences, but since the error variances add up (Eq. 1), the effect is most pronounced in the AATSR data, where the $\varepsilon^2_{\mathrm{satellite}}$ term is small. In the MODIS Aqua and Terra data the $\varepsilon^2_{\mathrm{satellite}}$ term is thus too large to recognize this effect, except when only quality flags 5 are used and solar elevation angles are below −5°.

The AMSR-E observations do not show a behavior similar to the IR products. We speculate, that this is due to the relatively large standard deviations of this system and the large spatial resolution of the MW observations, i.e. all observations within a 15 km distance are included in the footprint of the satellite observation.

4. General error statistics

Using the match-up data set, error statistics are derived for all the products. Table 2 shows the overall standard deviation and bias for each of the products and for quality flags 4 and 5 using match-up windows of 5 km and 90 min. The solar elevation angle of 0 is used to distinguish between day and night.

The table shows that nighttime satellite observations generally perform better than daytime observations. They have smaller absolute biases and standard deviations. One exception is AMSR-E observations that have smaller bias and lower standard deviation during the day as compared to the night. There are large differences in the

Table 2
Overall nighttime (upper) and day time (lower) error statistics (satellite-in situ) for the satellite products in the Arctic Ocean (>60° N). The numbers have been calculated using match-up windows of 5 km and 90 min and are given for satellite quality flags (QF) 4 and 5. Note that the MODIS Aqua and Terra data are only nighttime observations. The numbers in parenthesis for Metop_A show QF 4 statistics for the period June 2010 to Jan 2011, where both quality flags 4 and 5 observations were available.

Night	Number of matches		Bias		Std dev of errors	
Product	Qf 4	Qf 5	Qf 4	Qf 5	Qf 4	Qf 5
NAVO-GAC	977	8558	−0.02	−0.03	0.45	0.36
AATSR	4329	35,518	0.02	−0.08	0.48	0.36
Metop-A	95,553 (36,359)	13,120	−0.09 (−0.09)	−0.27	0.42 (0.47)	0.47
MODIS (Aqua)	210,273	312,415	−0.73	−0.14	1.42	0.70
MODIST (Terra)	166,990	270,939	−0.68	−0.10	1.47	0.69
AMSR-E	151,986	0	0.11	NA	0.76	NA
Day	**Number of matches**		**Bias**		**Std dev of errors**	
Product	Qf 4	Qf 5	Qf 4	Qf 5	Qf 4	Qf 5
NAVO-GAC	1918	12,891	−0.13	−0.01	0.49	0.36
AATSR	125	43,798	0.39	−0.27	0.44	0.47
Metop-A	215,490 (113,506)	29,693	0.33 (0.37)	0.05	0.45 (0.49)	0.40
MODIS (Aqua)	0	0	NA	NA	NA	NA
MODIST (Terra)	0	0	NA	NA	NA	NA
AMSR-E	142,282	0	0.04	NA	0.66	NA

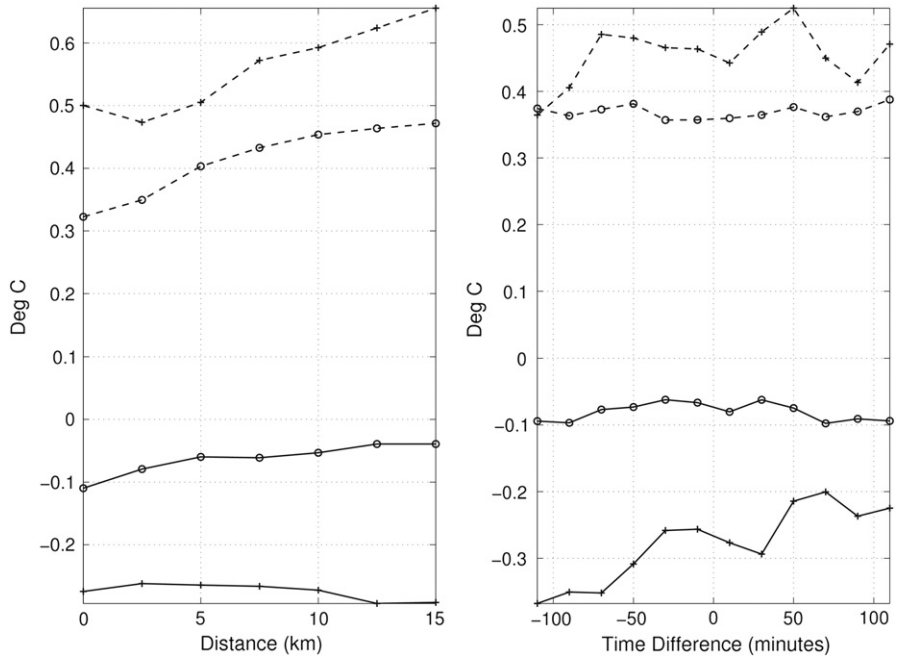

Fig. 3. Bias (solid) and standard deviation (dashed) of satellite-in situ observations for the AATSR observations as a function of the match-up distances Δx (left, for Δt<75 min) and Δt (right, for Δx 5 km). Circles indicate nighttime, and plus signs daytime observations. The binning interval is 2.5 km (left) and 20 min (right).

performance of the satellite products for the Arctic region. The AATSR, Metop-A and NAVO-GAC satellite products have small absolute biases and standard deviations lower than 0.5 °C for nighttime observations, whereas the MODIS Aqua and Terra and the AMSR-E products have higher standard deviations. Note that due to the absence of Metop-A quality flag 5 observations before June 2010, the errors are not representative for the full 15-month period. The impact of the quality flags 4 and 5 is different to each product. The majority of the products show slightly degraded, but still scientifically valid, satellite SST observations with quality flag 4, except for the MODIS Aqua and Terra products which have large errors both in terms of bias and standard deviation for quality flag 4. At high latitudes there are long periods with twilight conditions, which can be a challenge to the cloud masking. Therefore, the error statistics were examined for day, night and twilight conditions, using the solar elevation angles of −5 and 5° as the twilight interval (not shown). The general day/night error statistics showed a slight improvement (less than 0.04 °C in bias and less than 0.05 °C in standard deviation) when excluding the twilight match-ups. For most of the products, except AMSR-E, the error standard deviations for twilight conditions were higher than deviations for both day and night. MODIS Aqua and Terra observations showed the largest effect for low solar elevation angles, with twilight observations being 0.1–0.2 °C colder than nighttime observations.

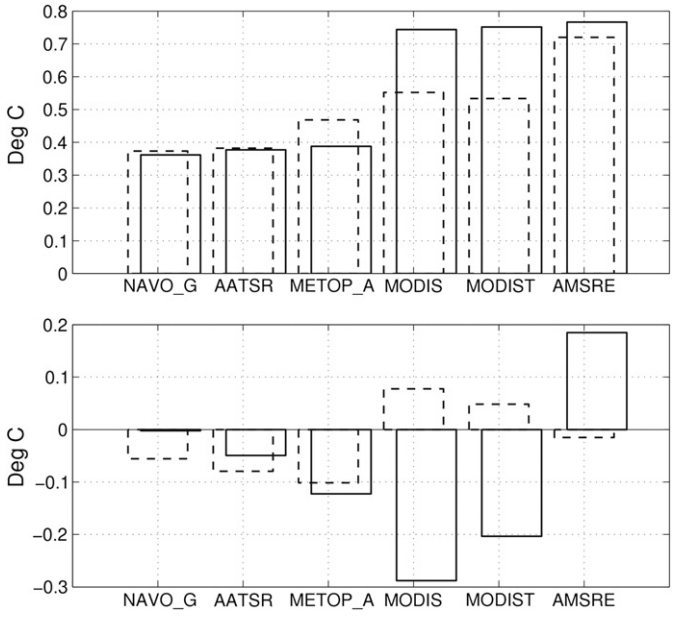

Fig. 4. Error statistics (satellite-in situ) for waters colder (solid) and warmer (dashed) than 5 °C. Upper figure shows standard deviation and lower figure shows bias.

In the rest of the paper, we will only consider MODIS Aqua and Terra quality flag 5 observations, whereas we will use quality flags 4 and 5 for all the other satellite products. If not otherwise stated, the match-up limits will be Δx of 5 km and Δt of 120 min. Due to the need for more match-ups when calculating detailed statistics for subsections of the dataset, the temporal limit is higher than the 90 min used to derive the Table 2 results.

As indicated in Fig. 2, most of the in situ observations are located within the Nordic seas, with SST of up to 15 °C in the Norwegian Sea. To validate the satellite products for colder conditions, the statistics were calculated separately for nighttime match-ups with temperatures below and above 5 °C as shown in Fig. 4.

For the AATSR, Metop-A and NAVO-GAC products, the performance in cold water does not differ significantly from warmer water performance across the entire domain. For the MODIS Aqua and Terra and the AMSR-E products, there is a significant bias difference between the performance in cold water and warmer water results.

The large annual cycles in atmospheric and oceanic conditions necessitates examination of the seasonal trends of the satellite products. Fig. 5 shows the monthly error statistics for the six different products. A minimum of 100 match-up pairs was required to calculate monthly bias and standard deviation. Note that since the MODIS Aqua and Terra products only contain nighttime data, the number of match-ups during the summer months is limited.

Fig. 5 shows points to significant seasonal biases in the Arctic. The Metop-A product has a warm bias of up to 0.4 °C during summer and a cold bias during the winter. The reason behind the warm Metop-A bias is being investigated, and preliminary results indicate, that it may be caused by moisture in the lower atmosphere (Le Borgne,

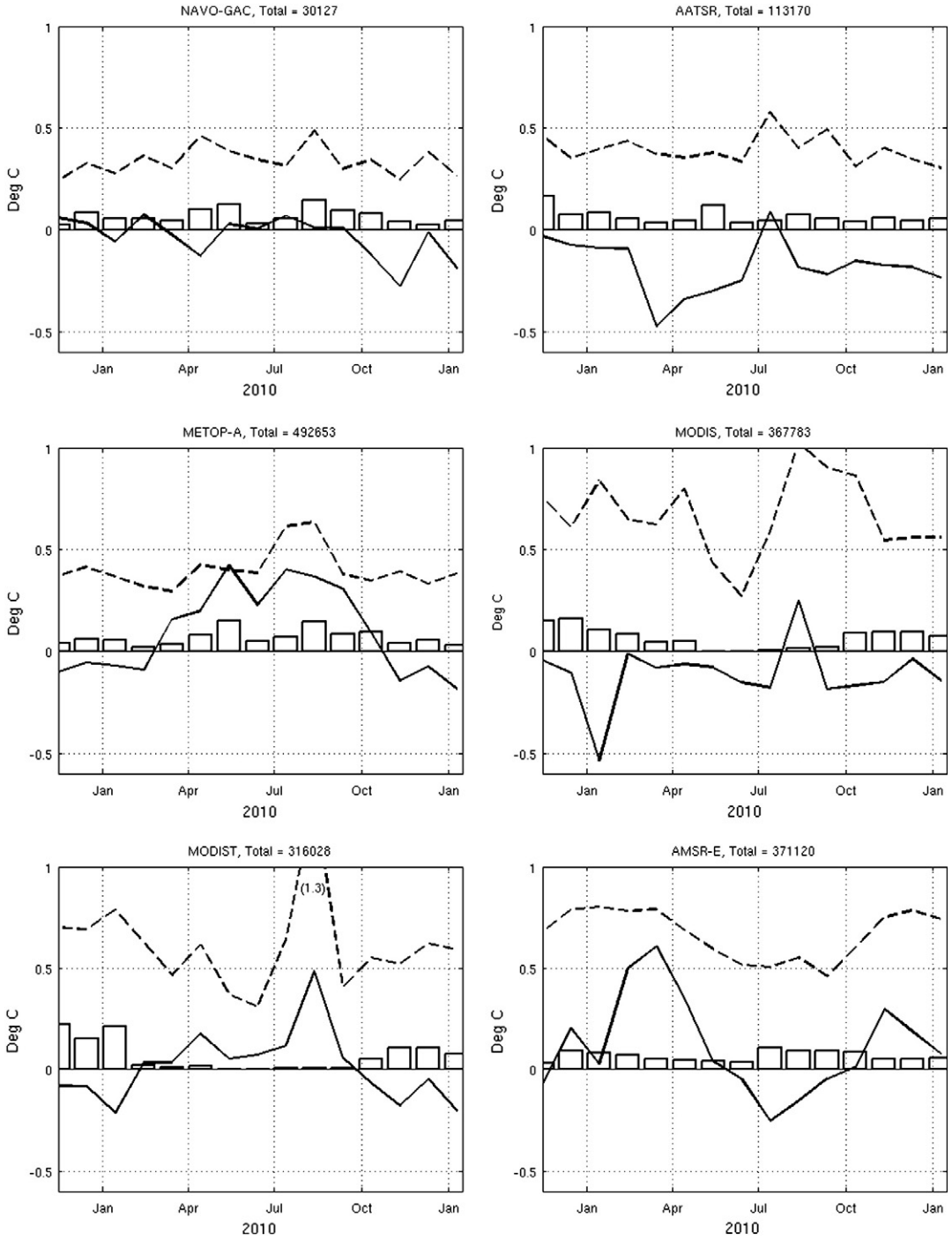

Fig. 5. Monthly mean bias (solid) and standard deviation (dashed) for the six satellite products. The bars indicate the normalized number of match-ups for each month and the total number appears from the title.

pers. Comm., 2011). The temporal Metop-A pattern in bias is almost opposite to the biases in the AMSR-E observations, with a cold bias during summer and a warm bias during spring and autumn. The seasonal bias trend in the AMSR-E observations is opposite to the bias trend in the Southern Ocean with positive austral summer biases (Dong et al., 2006). The AATSR and NAVO-GAC have small seasonal variations in the biases, and the standard deviations are nearly constant throughout the year. The good performance of the 9 km NAVO-GAC product is probably due to the averaging over many pixels and the very conservative cloud detection and quality control, where many observations are discarded (May et al., 1998). In addition, the calculation of the NAVO-GAC SSES biases is related to in situ observations and updated daily. There is no overlap between the in situ data used for validation and for SSES calculation. However, since the same buoy enters the validation and SSES correction, systematic errors on buoy observations might potentially be excluded from the error statistics. The SSES biases have been subtracted here, which might explain the absence of monthly or seasonal bias variations (May, pers. Comm., 2011).

To examine in more detail the significant seasonal variations in biases, the error statistics were calculated for solar elevation angles with an interval of 10° (Fig. 6).

Again, the NAVO-GAC observations show a very stable performance, which might be due to the in situ based SSES correction scheme. The AATSR satellite observations have a substantial negative bias for small

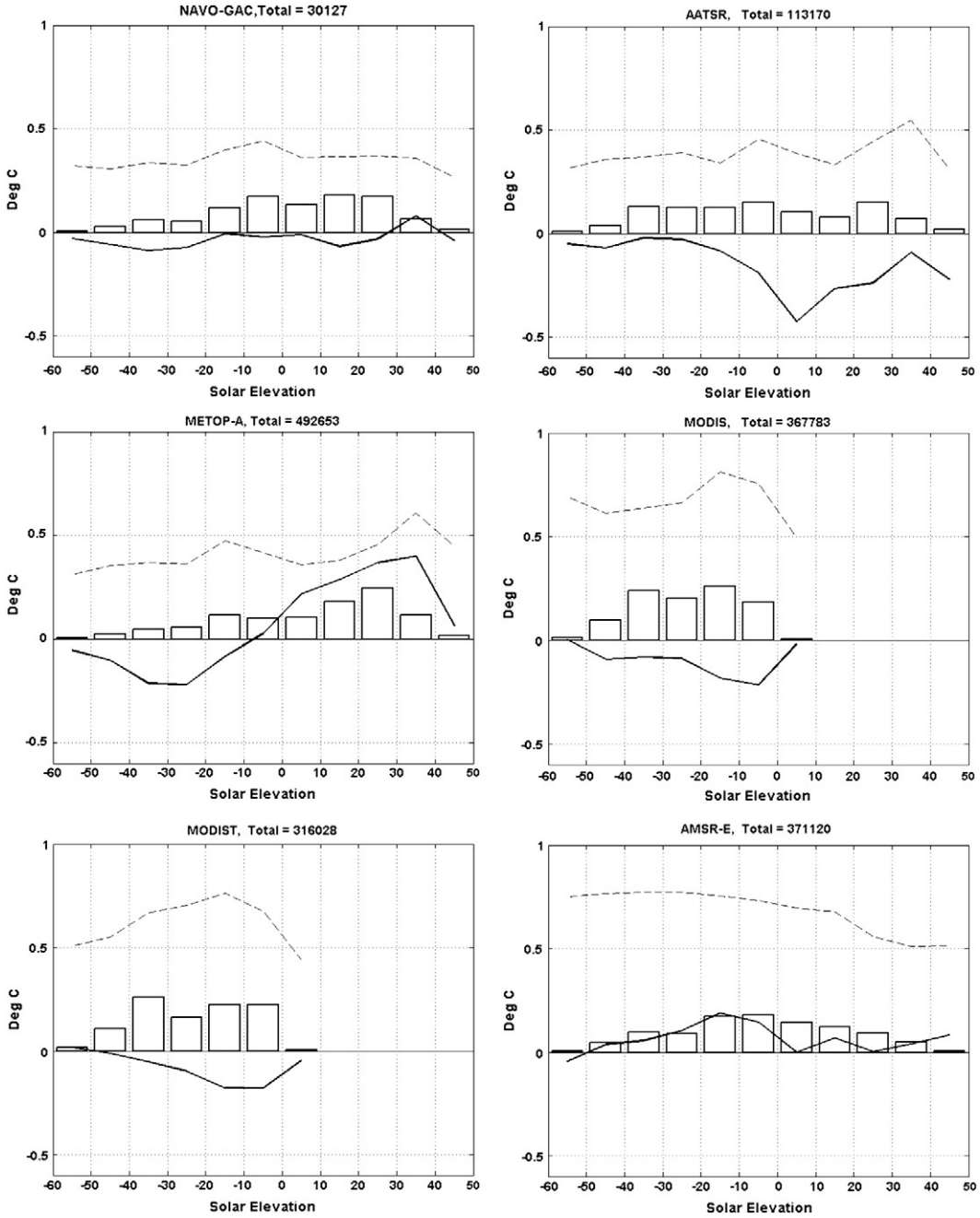

Fig. 6. Standard deviation (dashed) and Bias (solid) of the match-ups (satellite-in situ), as a function of solar elevation angle with an interval of 10°. The bars indicate the normalized number of observations in this solar angle interval, and the total number of observations is given in the title. Note that very few positive solar elevation angles are found for the nighttime MODIS Aqua and Terra observations.

absolute solar elevation angles, which may be related to undetected clouds during twilight conditions (Corlett, pers comm., 2011). The Metop-A data has a positive bias for solar elevation angles of more than 0° and a negative bias for solar elevation angles smaller than −10. This is in agreement with the findings in Poulter & Eastwood, 2008.

Both MODIS products indicate larger negative biases and enhanced standard deviation for solar elevation angles between −20 and 0°. The 10 °C difference threshold on the satellite-in situ match-ups, as mentioned in Section **3**, was important for the MODIS Aqua and Terra products when calculating statistics for the solar elevation intervals. A number of satellite observations with a very cold bias of −20 °C were present in both MODIS products for solar elevation angles between −10 and 10. The MODIS match-up dataset had 1700 and the MODIST product 203 erroneous quality flag 5 observations which would have resulted in significantly higher errors in Fig. 6, if they had not been excluded. The similarity between the performances of the two MODIS products indicates that this problem is probably a general MODIS problem arising from e.g. the cloud screening algorithm in twilight conditions. The AMSR-E biases are not related to solar elevation, but the error standard deviations for positive (daytime) solar elevation angles are significantly lower compared to the nighttime error standard deviations.

The results presented in Figs. 5 and 6 are due to the different observation techniques, the data processing and the cloud masking. A full investigation and explanation of all of the products and their error characteristics is beyond the scope of this paper, since its focus is on documenting and characterizing the errors for the individual products.

5. Error characteristics

When satellite SST observations are used for operational data assimilation, for climate data records or in merged and interpolated level 4 SST products, it is essential to specify the error scales of the satellite observations (e.g., Høyer & She., 2007; Reynolds & Smith, 1994). The 15-month match-up dataset described in the previous sections makes constitutes a good basis for an investigation of the different satellite error scales. Daily mean satellite errors on a 2° longitude and 1° latitude grid were computed for the full 15 months period using the match-up dataset described earlier. It is necessary to do the averaging over sufficient time and space to obtain satellite error time series with enough data to ensure robust correlation results. However, the spatial and temporal averaging scales should not be so large that it filters out the dominant noise present in the system.

5.1. Temporal scales of the errors

The daily averaged error fields were used for calculating the temporal autocorrelations of the error time series for each product, shown in Fig. 7.

The error correlations have only been calculated when at least 10 daily data pairs were available and when a minimum of 10 correlation estimates were available for a given lag. No results are available for the AATSR because of the narrow swath of the AATSR sensor results in very few grid points with daily mean errors. The figure shows that the temporal scale of the error correlations (the 1/e cross over) is about 1 to 2 days, with the AMSR-E product having the longest temporal scales and the MODIST having the shortest. As variability in the atmospheric conditions is the main contributor to the satellite errors, it was expected, that we find the error correlation scales to be on the order of a few days, which is similar to temporal scales of the weather (e.g., Peixoto & Oort, 1992). The "all-weather" AMSR-E observations provide a large number of match-up data.

5.2. Spatial scales of the errors

The daily averaged error time series were used to calculate correlation coefficients between time series in different grid points. A minimum of 10 pairs of observations were required to calculate the correlations, and all the correlation coefficients were arranged according to the distance between the two grid points. These results were averaged for every 200 km of separations, and an average correlation value was calculated for bins, where at least 5 correlation estimates were available. The results in Fig. 8 show that the spatial scales (1/e crossing point) of the satellite errors are on the order of 300 to 500 km.

The spatial scales are very similar for all the products. The good coverage of the AMSR-E sensor is evident again in Fig. 8 (right) which shows that the AMSR-E correlation results are based upon 10 times more correlation estimates than the other satellite products. The spatial scales of the IR satellite errors are smaller than the 600–800 km reported in Reynolds and Smith (1994) for lower latitudes and the general synoptic scale of the weather systems of 1000 km. This could be related to the low humidity in the Arctic and the weaker association between atmospheric water vapor and the differences in AVHRR channel 4 and 5 brightness temperatures (see e.g. Kumar et al., 2003). With a reduction in these large scale errors, other error contributions with smaller spatial scales such as erroneous cloud detection and sub-pixel clouds could have a larger influence on the results.

5.3. Correlation of satellite errors

Other studies have used the AATSR observations to assess the quality of other SST sensors, because of its high accuracy (Corlett et al., 2006; O'Carroll et al., 2006; Noyes et al., 2006; Robinson, 2004; Stark et al., 2008). However, the AATSR based correction method does not work well in the Arctic Ocean due to the small number of observations in persistent cloudy conditions. In addition, the dependence upon an old satellite sensor, launched in 2002 and with a nominal lifetime of 5 year, is a critical weakness for systems that require quality data every day. However, for a multi sensor approach, it is essential to know the error characteristics of each of the satellites, and that the errors on the satellite products are not highly correlated. To examine the correlation of the satellite errors, daily averaged differences as described above were used. A minimum of 5 common daily error values was required before a correlation was calculated and at least 20 correlation estimates before an average correlation was calculated. The results are shown in Fig. 9. Not enough observations were available to calculate correlations between AATSR and NAVO-GAC, MODIS Aqua and Terra.

Fig. 9 shows that the AMSR-E MW errors have a low correlation (<0.23) with the IR errors. This is as expected since the IR and MW satellite errors are caused by different atmospheric effects, as discussed earlier. Within the IR products, the differences are correlated with the highest correlations between the same instruments. There are elevated error correlations between SST products from the same sensor, such as AVHRR (Metop-A versus NAVO-GAC) of 0.52 and MODIS (Aqua and Terra) of 0.40. This is as expected since the same types of instruments typically have common error characteristics. The AATSR errors have low correlation with the other products. However, there are insufficient data for reliable correlation with several of the other products. The results indicate that for referencing the satellite against each other and for constructing a multi sensor merged product, the AMSR-E data provide independent information that may improve the results. Until now, this potential has not been fully exploited due to the imperfect MW error characterization, an area where more work is needed.

6. Marginal ice zone effects

The seasonal ice cover in the Arctic is about 10 million km^2 (Parkinson et al., 1999) and the position of the marginal ice zone (MIZ) varies substantially during the year, as evident from Fig. 1. Previous studies from the North Water Polynya (NOW) indicate, that the traditional IR algorithms in the marginal ice zone overestimate the SST by more than 2 °C on average, when they use the observed

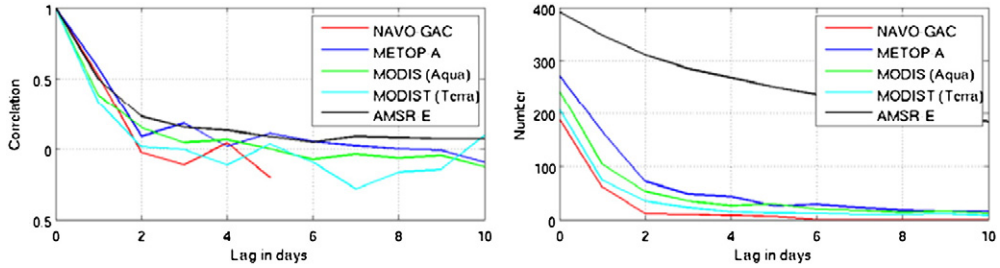

Fig. 7. Mean correlation of the daily errors, as a function of the lag in days (left). Number of correlation estimates available for averaging time series (right).

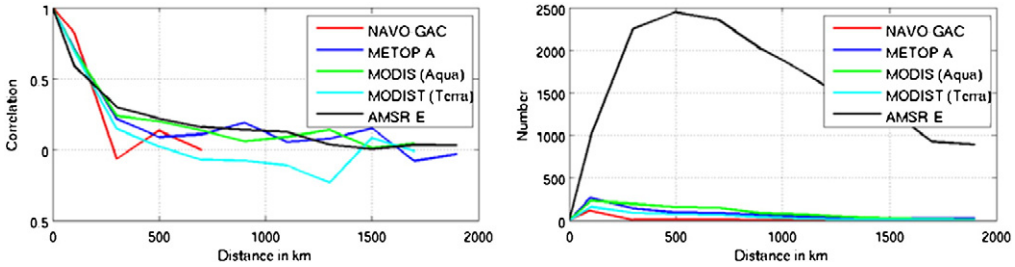

Fig. 8. Correlations of the errors on the satellite products as a function of separation distance (left) and number of correlation estimates available for the average products (right). The results have been averaged for 200 km intervals.

AVHRR channel 4 and 5 difference in brightness temperature to correct for water vapor, as in global IR algorithms (Vincent et al., 2008a, 2008b). These studies were limited to the NOW and covered observations from April to July, with the largest overestimation in the beginning of the period. Moreover, most of the satellite products do not use ice information in their data processing but rely on gross error checks or cloud masks to discard or flag ice contaminated observations. An exception from this is the Metop-A algorithm, which uses an observation driven Bayesian classifier (Eastwood & Andersen, 2007). With the match-up dataset presented here, more general error statistics from the marginal ice zone can be derived from a larger area and for several IR and MW products.

As described in Section **3**, a minimum distance to the ice edge has been assigned to all satellite versus in situ pairs. To examine the performance of the satellite products in the vicinity of the ice edge, the ice distance information has been used for calculating the mean bias and standard deviation for each product as a function of the distance from the ice edge, averaged in 25 km intervals. The results are shown in Fig. 10, where bars indicate the normalized number of match-ups used for the interval. The total number of match-ups is given for each SST product.

Several of the global satellite products perform well in the vicinity of the Ice edge. The MODIS Aqua and Terra products appear to have significantly higher error standard deviations within 150 km off the ice, compared to the overall and cold water statistics reported earlier (Table 2 and Fig. 4). The AMSR-E bias within 25 km from the ice edge appears to be substantially warmer than further away from the ice edge. This might be due to the large footprint of the 6.9 GHz channel, note however that these results are based upon only 170 match-up pairs. There is an indication that the AATSR observations have larger errors near the ice edge. This effect is seen for both day and night observations and could be due to the lack of external and internal ice information in the AATSR data processing. Considering the number of available data and the error statistics, it appears that the Metop-A observations provide the best products in the marginal ice zone, with a good data return and a relatively uniform validation result when the ice is approached. This might be related to the Bayesian classifier that allows a more accurate ocean and ice classification.

The high latitude SST overestimation demonstrated by Vincent et al., (2008a), (2008b) by several °C is not confirmed here, some of the products even show a decrease in the bias within the last 25 km from the ice edge. Note however, as seen in Fig. 2, that no in situ observations were available from the Baffin Bay and NOW, where the atmospheric conditions can be much colder and drier than in the Nordic seas, where most of the match-ups for this study are obtained. In addition, stricter match-up criteria were used to derive the match-ups, and the in situ observations were provided by the Marine-Atmosphere-Emitted Radiance Interferometer (M-AERI) instrument (Kearns et al., 2000).

7. Conclusions

The validation of the global satellite SST products in the Arctic showed that the distance between the observations is important when comparing satellite and in situ observations in this region. Increasing the distance from 5 to 15 km increases the standard deviation of the satellite versus in situ differences for the AATSR from 0.32 to 0.47 for nighttime comparisons. This influence of spatial match-up distance is significant and can be explained by the large temperature gradients in the Nordic seas and Barents Sea, where the majority of the match-ups are located. In addition, the Rossby

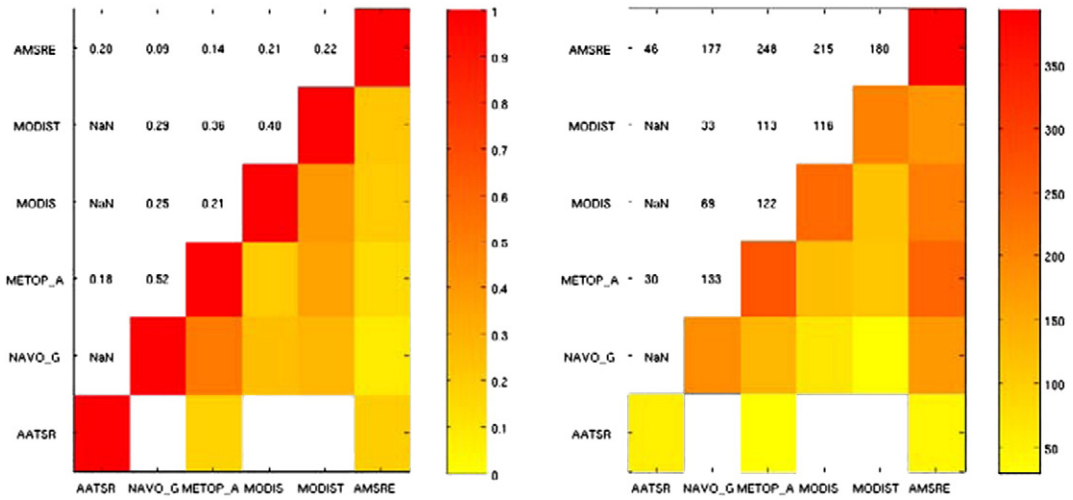

Fig. 9. Correlation of satellite errors between the different SST products (left). Total number of satellite-versus in situ pairs that went into the correlation calculation (right). White spaces indicate that no correlations were calculated. The correlation numbers are printed in the upper part of the matrices and shown in colors in the lower part.

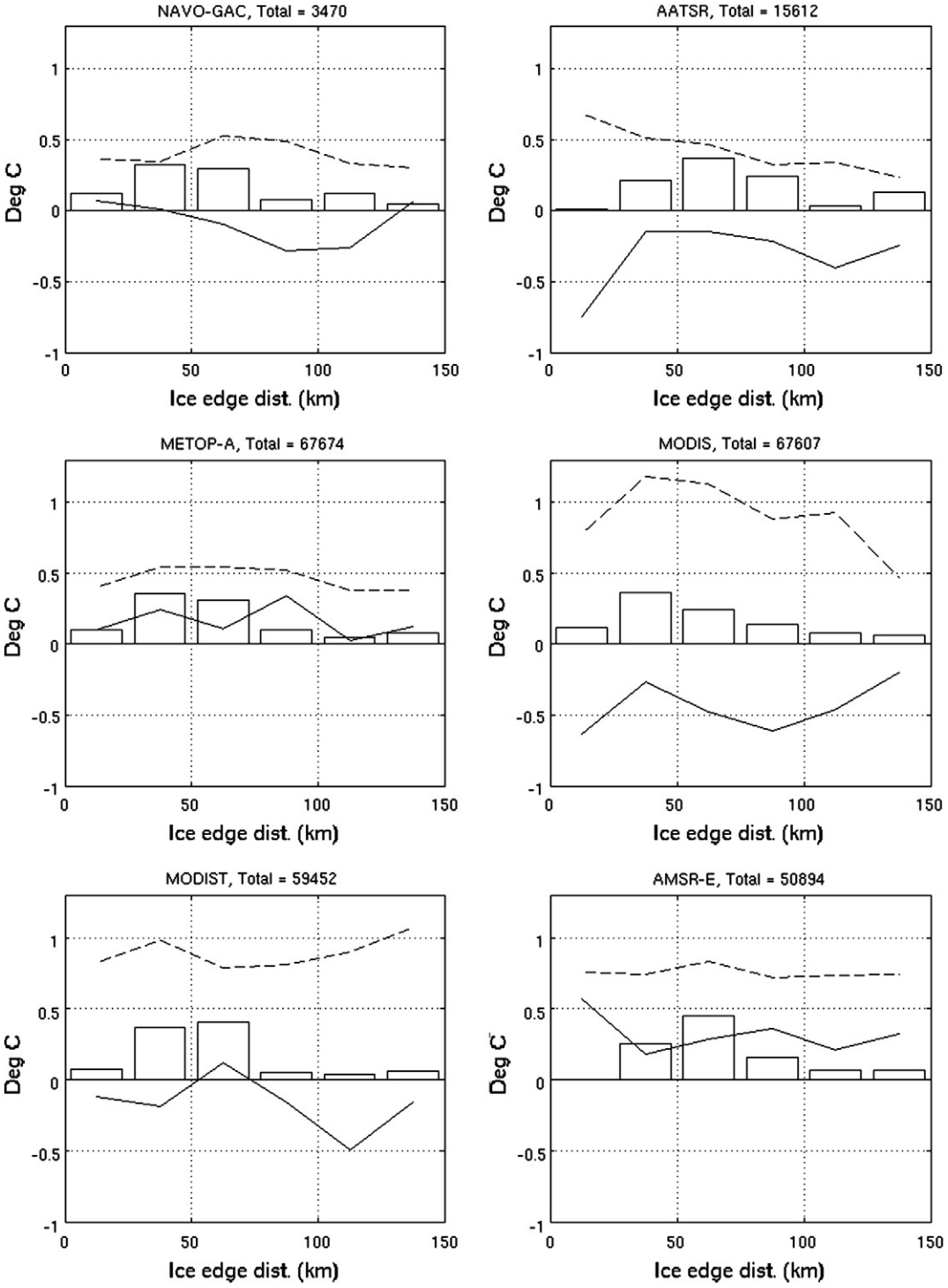

Fig. 10. Marginal ice zone SST bias (solid) and standard deviation (dashed) of nighttime satellite-in situ observations as a function of distance from the ice edge, calculated for every 25 km. Only statistics with more than 100 observations are shown.

radius and the scales of the ocean eddies are small at high latitudes, which introduces SST variability in the order of 10 km.

The most accurate satellite observations are obtained with IR satellite observations from either the AVHRR (NAVO-GAC) or the AATSR, which show relatively stable seasonal bias and low standard deviations. The Metop-A observations appear to have a summer bias of 0.3–0.4 °C. In general, the results from this study show that the IR satellite observations in the Arctic Ocean are of good quality, but the data are sparse due to a persistent cloud cover. The MODIS Aqua and Terra nighttime products have larger errors in the Arctic Ocean than the other IR products, and their performance degrades significantly when using quality flags lower than 5.

The large potential of the MW observations from the AMSR-E sensor to provide independent information is evident throughout the study. The number of match-up data available for validation of AMSR-E is very high despite the coarse spatial resolution. In addition, the daily errors of the satellite products are not highly correlated with the IR sensor products, and the AMSR-E thus gives independent SST estimates. Unfortunately, there are positive biases in the study region of more than 0.5 °C for several months during spring, and the bias for cold water

observations (SST < 5 °C) is substantially larger than for warmer SSTs. The origin of these biases is unknown at present (Gentemann, personal comm., 2011) and demonstrates the need for future work on MW SST error characterization.

Other types of in situ observations could be included in future studies to enhance the number of match-ups. However, the buoys have very good quality data and including other types of observations, such as ship observations with poorer quality will introduce noise. The need for more in situ observations is pronounced in the seasonal open water regions in the Russian part of the Arctic Ocean and in the Baffin Bay. As seen in Fig. 2, most of the in situ observations are from the Nordic seas, Barents Sea and Chukchi Sea.

Acknowledgments

We thank the three anonymous reviewers for their constructive comments to the manuscript. We thank the Naval Oceanographic Office, ESA UK-MM-PAF, EUMETSAT OSI SAF, NASA JPL and Remote Sensing Systems for providing the data. This study received financial support from the Danish Agency for Science, Technology and Innovation and is a part of the Greenland Climate Research Centre. Financial support was also received from the MyOcean project, which has been funded by the European Commission under the FP7 space program.

References

Barton, I. J. (1995). Satellite-derived sea surface temperatures: Current status. *Journal of Geophysical Research*, *100*(C5), 8777–8790, doi:10.1029/95JC00365.

Brown, O. B., Minnett, P. J., Evans, R., Kilpatrick, K., Kumar, A., Sikorski, R., et al. (1999). *MODIS infrared sea surface temperature algorithm, algorithm theoretical basis document.* Version 2.0, University of Miami, NAS5-31361.

Carton, J. A., Chepurin, G., Cao, X., & Giese, B. (2000). A simple ocean data assimilation analysis of the global upper ocean 1950–95. Part I: Methodology. *Journal of Physical Oceanography*, *30*, 294–309.

Casey, K. S., & Cornillon, P. (1999). A comparison of satellite and *in situ* based sea surface temperature climatologies. *Journal of Climate*, *12*(6), 1848–1863.

Chan, P. -K., & Gao, B. -C. (2005). A comparison of MODIS, NCEP and TMI sea surface temperature datasets. *IEEE Geoscience and Remote Sensing Letters*, *2*(3), 270–274.

Comiso, J. C., Parkinson, C. L., Gersten, R., & Stock, L. (2008). Accelerated decline in the Arctic sea ice cover. *Geophysical Research Letters*, *35*, L01703, doi:10.1029/2007GL031972.

Corlett, G. K., Barton, I. J., Donlon, C. J., Edwards, M. C., Good, S. A., Horrocks, L. A., et al. (2006). The accuracy of SST retrievals from AATSR: An initial assessment through geophysical validation against *in situ* radiometers, buoys and other SST data sets. *Advances in Space Research*, *37*(4), 764–769, doi:10.1016/j.asr.2005.09.037 Natural Hazards and Oceanographic Processes from Satellite Data, ISSN 0273–1177.

Dong, S., Gille, S. T., Sprintall, J., & Gentemann, C. (2006). Validation of the Advanced Microwave Scanning Radiometer for the Earth Observing System (AMSR-E) sea surface temperature in the Southern Ocean. *Journal of Geophysical Research*, *111*, C04002, doi:10.1029/2005JC002934.

Donlon, C. J., Minnett, P. J., Gentemann, C., Nightingale, T. J., Barton, I. J., Ward, B., et al. (2002). Toward improved validation of satellite sea surface skin temperature measurements for climate research. *Journal of Climate*, *15*, 353–369.

Donlon, C., Robinson, I., Casey, K. S., Vazquez-Cuervo, J., Armstrong, E., Arino, O., et al. (2007). The global ocean data assimilation experiment high-resolution sea surface temperature pilot project. *Bulletin of the American Meteorological Society*, *88*(8), 1197–1213, doi:10.1175/BAMS-88-8-1197.

Donlon, C., Casey, K., Gentemann, C., LeBorgne, P., Robinson, I., Reeynolds, R., et al. (2010). Successes and challenges for the modern sea surface temperature observing system. In J. Hall, D. E. Harrison, & D. Stammer (Eds.), *Proceedings of the "OceanObs'09: Sustained Ocean Observations and Information for Society" Conference (Vol. 2), Venice, Italy, 21–25 September 2009.* : ESA Publication WPP-306.

Eastwood, S., & Andersen, S. (2007). Masking of sea ice for Metop SST retrieval. OSI-SAF report. http://saf.met.no/docs

Eastwood, S., Le Borgne, P., Péré, S., & Poulter, D. (2011). Diurnal variability in sea surface temperature in the Arctic. *Remote Sensing of Environment*, doi:10.1016/j.rse.2011.05.015.

Embury, O., Merchant, C., & Corlett, G. (2012). A reprocessing for Climate of Sea Surface Temperature from the Along-Track Scanning Radiometers: Initial Validation, accounting for skin and diurnal variability effects. *Remote Sensing of Environment, 116*, 62–78, doi:10.1016/j.rse.2011.02.028.

Emery, W. J., & Thomson, R. E. (1998). *Data analysis methods in physical oceanography.* : Pergamon Elsevier Science 400 pp..

Emery, W. J., Baldwin, D. J., Schlüssel, P., & Reynolds, R. W. (2001). Accuracy of *in situ* sea surface temperatures used to calibrate infrared satellite measurements. *Journal of Geophysical Research*, *106*, 2387–2405, doi:10.1029/2000JC000246.

Gentemann, C. L., Minnett, P. J., Le Borgne, P., & Merchant, C. J. (2008). Multi-satellite measurements of large diurnal warming events. *Geophysical Research Letters*, *35*, L22602, doi:10.1029/2008GL035730.

Gentemann, C. L., Meissner, T., & Wentz, F. J. (2010). Accuracy of satellite sea surface temperatures at 7 and 11 GHz. *IEEE Transactions*, *48*(3).

Harris, A. R., & Saunders, M. A. (1996). Global validation of the along-track scanning radiometer against drifting buoys. *Journal of Geophysical Research*, *101*(C5), 12,127–12,140, doi:10.1029/96JC00317.

Høyer, J. L., & She, J. (2007). Optimal interpolation of sea surface temperature for the North Sea and Baltic Sea. *Journal of Marine Systems*, *65*(1–4), 176–189.

Kearns, E. J., Hanafin, J. A., Evans, R. H., Minnett, P. J., & Brown, O. B. (2000). An independent assessment of Pathfinder AVHRR sea surface temperature accuracy using the Marine Atmosphere Emitted Radiance Interferometer. *Bulletin Meteorological Society*, *81*, 1525–1536.

Kumar, A., Minnett, P. J., Podestá, G., & Evans, R. H. (2003). Error characteristics of the atmospheric correction algorithms used in retrieval of sea surface temperatures from infrared satellite measurements: Global and regional aspects. *Journal of Atmospheric Science*, *60*, 575–585.

Lindsay, R. W., & Zhang, J. (2005). The thinning of Arctic sea ice, 1988–2003: Have we passed a tipping point? *Journal of Climate*, *18*, 4879–4894.

May, D. A., Parmeter, M. M., Olszewski, D. S., & McKenzie, B. D. (1998). Operational processing of satellite sea surface temperature retrievals at the Naval Oceanographic Office. *Bulletin of the American Meteorological Society*, *79*, 397–407.

McClain, E. P., Pichel, W. G., & Walton, C. C. (1985). Comparative performance of AVHRR-based multichannel sea surface temperatures. *Journal of Geophysical Research*, *90*(C6), 11,587–11,601, doi:10.1029/JC090iC06p11587.

Merchant, C. J., Harris, A. R., Murray, M. J., & Zavody, A. M. (1999). Toward the elimination of bias in satellite retrievals of sea surface temperature 1. Theory, modelling and inter-algorithm comparison. *Journal of Geophysical Research*, *104*, 23565–23578.

Noyes, E. J., Minnett, P. J., Remedios, J. J., Corlett, G. K., Good, S. A., & Llewellyn-Jones, D. T. (2006). The accuracy of the AATSR sea surface temperatures in the Caribbean. *Remote Sensing of Environment*, doi:10.1016/j.rse.2011.02.028.

O&SI SAF project team (2010). *Low Earth Orbiter Sea Surface Temperature product user manual, version 2.2. Prepared by Météo France.*

O'Carroll, A. G., Eyre, J. R., & Saunders, R. W. (2008). Three-way error analysis between AATSR, AMSR-E, and *in situ* sea surface temperature observations. *Journal of Atmospheric and Oceanic Technology*, *25*, 1197–1207.

O'Carroll, A. G., Watts, J. G., Horrocks, L. A., Saunders, R. W., & Rayner, N. A. (2006). Validation of the AATSR Meteo product sea surface temperature. *Journal of Atmospheric and Oceanic Technology*, *23*, 711–726.

Parkinson, C. L., Cavalieri, D. J., Gloersen, P., Zwally, H. J., & Comiso, J. C. (1999). Arctic sea ice extents, areas, and trends, 1978–1996. *Journal of Geophysical Research*, *104*, 20 837–20 856.

Peixoto, J. P., & Oort, A. H. (1992). *Physics of climate.* : American Institute of Physics 520 pp.

Poulter, D. J. S., & Eastwood, S. (2008). *Validation of the OSI SAF Metop SST product in polar regions.* OSI-SAF report.

Rayner, N. A., Parker, D. E., Horton, E. B., Folland, C. K., Alexander, L. V., Rowell, D. P., et al. (2003). Global analyses of sea surface temperature, sea ice, and night marine air temperature since the late nineteenth century. *Journal of Geophysical Research*, *108*(D14), 4407, doi:10.1029/2002JD002670.

Reynolds, R. W., & Smith, T. M. (1994). Improved global sea surface temperature analyses using optimum interpolation. *Journal of Climate*, *7*, 929–948.

Robinson, I. S. (2004). Measuring the oceans from space: The principles and methods of satellite oceanography. Springer Praxis Ed. 669 pp.

Schluessel, P., Shin, H. -Y., Emery, W. J., & Grassl, H. (1987). Comparison of satellite-derived sea surface temperatures with *in situ* skin measurements. *Journal of Geophysical Research*, *92*(C3), 2859–2874, doi:10.1029/JC092iC03p02859.

Stark, J. D., Donlon, C., O'Carroll, A. G., & Corlett, G. (2008). Determination of AATSR biases using the OSTIA SST analysis system and a matchup database. *Journal of Atmospheric and Oceanic Technology*, *25*(7), 1208–1217.

Tomczak, M., & Godfrey, J. S. (1994). *Regional oceanography: An introduction.* New York: Pergamon 422 pp.

Vincent, R. F., Marsden, R. F., Minnett, P. J., Creber, K. A. M., & Buckley, J. R. (2008). Arctic waters and marginal ice zones: A composite Arctic sea surface temperature algorithm using satellite thermal data. *Journal of Geophysical Research*, *113*, C04021, doi:10.1029/2007JC004353.

Vincent, R. F., Marsden, R. F., Minnett, P. J., & Buckley, J. R. (2008). Arctic waters and marginal ice zones: 2. An investigation of arctic atmospheric infrared absorption for advanced very high resolution radiometer sea surface temperature estimates. *Journal of Geophysical Research*, *113*, C08044.

Walsh, J. E., Kattsov, V. M., Chapman, W. L., Govorkova, V., & Pavlova, T. (2002). Comparison of Arctic climate simulations by uncoupled and coupled global models. *Journal of Climate*, *15*, 1429–1446.

Walton, C. C., Pichel, W. G., Sapper, J. F., & May, D. A. (1998). The development and operational application of nonlinear algorithms for the measurement of sea surface temperatures with the NOAA polar-orbiting environmental satellites. *Journal of Geophysical Research*, *103*, 27,999–28,012.

Wentz, F. J., & Meissner, T. (2000). *AMSR ocean algorithm theoretical basis document, version 2.* Santa Rosa, CA: Remote Sensing Systems.

Wentz, F. J., & Meissner, T. (2007). Supplement 1, Algorithm theoretical basis document for AMSR-E ocean algorithms. *Rss Tech Report 051707*. Santa Rosa, CA: Remote Sensing systems.

Wentz, F. J., Gentemann, C. L., Smith, D. K., & Chelton, D. B. (2000). Satellite measurements of sea-surface temperature through clouds. *Science*, *288*, 847–850.

Zavody, A. M., Mutlow, C. T., & Llewellyn-Jones, D. T. (1995). A radiative transfer model for SST retrieval for the ATSR. *Journal of Geophysical Research*, *100*, 937–952.